Ab initio potentials for the S(^3P_j)–rare gas dimers: Implementation for elastic and inelastic collisions and comparison with scattering potentials

J. Kłos[a] and G. Chałasiński[b]
Faculty of Chemistry, Warsaw University, Pasteura 1, 03-093 Warszawa, Poland

Roman V. Krems
Harvard-Smithsonian Center for Astrophysics, Cambridge, Massachusetts 02138

A. A. Buchachenko
Department of Chemistry, Moscow State University, Moscow 119899, Russia

Vincenzo Aquilanti and Fernando Pirani[c]
Dipartimento di Chimica, Università di Perugia, 06123 Perugia, Italy

David Cappelletti[c]
Dipartimento di Ingegneria Civile ed Ambientale, Università di Perugia, 06125 Perugia, Italy

(Received 4 February 2002; accepted 13 March 2002)

The interaction potentials between the ground state S(^3P) atom and rare gas atoms Rg (He, Ne, Ar, Kr, and Xe) in $^3\Pi$ and $^3\Sigma^-$ states are calculated *ab initio* using an unrestricted CCSD(T) level of theory and extended correlation consistent basis sets augmented by bond functions. For NeS, the effects of extending the basis set, of a more accurate treatment of triple excitations within the coupled cluster method, and of the frozen core approximation are analyzed. The spin–orbit interaction is taken into account by the commonly used atomic model, whose validity is verified by the direct *ab initio* calculations of spin–orbit coupling matrix elements. The *ab initio* potentials are tested in the calculations of the absolute total scattering cross sections measured in molecular beams and compared with the potentials derived from the same data. This comparison, along with an analysis in terms of correlation formulas, proves the high accuracy of *ab initio* potentials and characterizes the sensitivity of scattering cross sections to the properties of interaction potentials. Both *ab initio* and scattering derived potentials are implemented in the study of inelastic fine structure transitions in S+Rg collisions. The relaxation rate constants are calculated and compared with those for O+Rg collisions. © *2002 American Institute of Physics.*
[DOI: 10.1063/1.1476009]

I. INTRODUCTION

Studies of intermolecular interactions are important in order to understand transport and relaxation phenomena induced by collisions in the gas phase, to model the structure and dynamics of clusters and condensed phases, and to gain a deeper insight into the nature of the chemical bond. The role of open-shell and fine structure effects (in particular the spin–orbit coupling) is central for processes such as collisional energy redistribution in plasmas, in discharges, in laser media. It is thus not surprising that several researchers focused their attention on the accurate description of interactions in systems involving open-shell atoms. The analysis of such interactions is of special interest because it allows one to investigate the open-shell anisotropy which manifests itself in the splitting of degenerate electronic states of the open-shell atom upon the interaction with an external particle. At large internuclear distances this splitting reflects mainly the nonspherical electron density distribution of a free open-shell atom. By way of contrast, factors of chemical nature (which may be related to electron charge-transfer stabilization pertinent to formation of the incipient chemical bond) determine the interaction anisotropy at short and intermediate distances. Systematic investigations of the various sources of anisotropies in such systems can thus bridge the gap between the van der Waals interaction and chemical binding, and provide a better understanding of how the chemical bond is formed.

There are several approaches to the accurate modeling of weak interatomic interaction potentials (here ''weak'' means between 0.1 and 10 kJ/mol—a few hundreds of wave numbers or less). On the experimental side, interaction potentials can be obtained from the analysis of cross section data from molecular beam scattering experiments. Differential and integral elastic cross sections, in particular if quantum interference effects are observed in a sufficiently wide collision velocity range, are very sensitive to the position of the repulsive wall, to the well region area, and to the long-range attraction.[1] As is well known, the potential well is deter-

[a]Present address: Institute of Theoretical Chemistry, NSRIM, University of Nijmegen, Toernooiveld 1, 6525 ED Nijmegen, The Netherlands.
[b]Also at Chemistry Department, Oakland University, Rochester, Michigan 48309.
[c]Also at INFM, Unità di Perugia, 06123 Perugia, Italy.

mined by a delicate balance between long-range attraction and short-range repulsion forces. For open-shell atoms the collision dynamics can be considered as governed by a manifold of coupled potentials,[2] and this may lead to some additional subtleties in the analysis of the experimental results. A statistical distribution of the internal states of the open-shell species has been usually assumed in the analysis of scattering experiments.[3,4] A more sophisticated alternative involves the use of state selection techniques: magnetic field analysis[5] represents a most advanced tool among the approaches used so far. Recent examples, pertinent also to the present study, have included the accurate experimental determination of $O(^3P_j)-Rg$,[6] $F(^2P_j)-Rg$,[7,8] and $Cl(^2P_j)-Rg$ (Ref. 9) interactions (with Rg=He, Ne, Ar, Kr, and Xe).

Spectroscopic measurements provide complementary information on the interaction potentials for weakly bound systems, usually in the region of the potential well. They can encounter difficulties when applied to studies of the lower lying electronic states in the diatomic complexes involving open-shell atoms. Due to the weak binding, it is difficult to generate the species in concentrations high enough to obtain well-resolved excitation spectra. Measurements of bound-free laser induced fluorescence are more instructive in this context (see, e.g., Refs. 10–12). However, selection rules do not usually allow the experiments to probe all the states correlating with the first dissociation limit, and therefore the anisotropy of interaction cannot be investigated in full details. Very accurate potentials have also been obtained from the analysis of microwave spectra for dimers involving open-shell cations (see, for example, Ref. 13), but only for the ground electronic states. Photoelectron spectroscopy of weakly-bound anions is yet another powerful alternative, especially the high-resolution zero electron kinetic energy (ZEKE) spectroscopy (see, e.g., Refs. 14–16). Because of the higher binding energy of anions and less strict selection rules, this approach is very promising and should be widely explored in the near future.

Since each experimental technique usually gives information limited to specific ranges of intermolecular distances and energies, the best atom–atom interaction potentials so far are those obtained by a multiproperty fit to various experimentally measured properties.[8,9,17–19]

One important direction is the implementation of empirical or semiempirical approaches which allows one to predict the binding properties of a system from the known properties of its fragments or analogous systems, often combining experimental information and theoretical considerations.[20–24] Indeed, a current issue of modern quantum chemistry is to assess how accurately the interaction potentials of weakly bound complexes can be computed by means of various methods of electronic structure theory.

Regarding the computation of interaction potentials from first principles, the calculations for weakly-bound open-shell systems are still considered as the state-of-the-art level of *ab initio* theories,[25] although many authors proved them to be feasible and accurate for a number of systems. In particular, recent highly accurate *ab initio* studies have been devoted to systematic analysis of RgCl (Refs. 26, 27) and RgO (Refs. 28–30) neutrals and anions.[27,28,31] Interaction potentials calculated in these works have been carefully tested against available experimental data, including the beam scattering and anion photoelectron ZEKE spectroscopy.

In the present paper we extend the application of the *ab initio* approach to RgS systems. The only experimental source of information on the interaction potentials of rare gas sulfides are the total integral scattering cross sections measured recently from molecular beam scattering for all Rg atoms except He.[32] These data have been analyzed in order to obtain the interaction potentials (hereafter referred to as *scattering* potentials). Previous *ab initio* calculations for the heavy KrS (Ref. 33) and XeS (Ref. 34) systems have been mainly designed to treat the states correlating with excited atomic limits and do not provide an accurate description of low-lying electronic states. Only very recently reliable *ab initio* HeS potentials have become available.[35]

The purposes and plan of the present paper are: (i) to evaluate accurate *ab initio* potentials for RgS systems (Rg =He–Xe) and to test the accuracy of the atomic model for spin–orbit coupling (Sec. II); (ii) to test the accuracy of the *ab initio* potentials on the scattering data (Sec. III); (iii) to compare the main features of the *ab initio* results with the potentials determined both by direct fitting the scattering data[32] and by means of the empirical correlation formulas recently developed[23,24] (Sec. IV); (iv) to investigate the dynamics of intramultiplet mixing in $Rg+S(^3P_j)$ inelastic collisions and to make a qualitative comparison with the results obtained previously for the $Rg+O(^3P_j)$ collisions[29,30] (Sec. V). Conclusions follow in Sec. VI.

II. CALCULATION OF THE *AB INITIO* INTERACTION POTENTIALS

A. *Ab initio* and fitting procedures

In the nonrelativistic approximation, the interaction of an $S(^3P)$ atom with a rare gas atom gives rise to two states of $^3\Pi$ and $^3\Sigma^-$ symmetry, whose potentials are designated as V_Π and V_Σ. Their electronic configurations are $p_x^2p_y^1p_z^1$ and $p_x^1p_y^1p_z^2$, respectively. The z axis is oriented along the Rg–S direction, so in the Σ state the Rg atom sees a doubly-occupied p-orbital, allowing a two-electron, closed-shell-like contact; to a first approximation, the interaction in this case can be considered as a purely van der Waals bonding between two closed-shell atoms. On the contrary, in the $^3\Pi$ state the Rg atoms make a one-electron open-shell contact with the singly occupied p-orbital of sulfur atom. Electron transfer leading to the stabilizing contributions from incipient bonding or charge transfer takes place. This chemical stabilization increases the $^3\Pi$ interaction energy and, in addition to the nonspherical electron density distribution of the sulfur atom affecting the long-range van der Waals interaction, is a main source of the interaction anisotropy, defined as the difference between $^3\Pi$ and $^3\Sigma^-$ potentials.

To calculate the potentials, the supermolecular approach is used. The interaction energy between sulfur and Rg (Rg =He, Ne, Ar, Kr and Xe) atoms is expressed as

$$\Delta E(R)=E_{\mathrm{RgS}}(R)-E_{\mathrm{Rg}}^{\mathrm{DCBS}}(R)-E_{\mathrm{S}}^{\mathrm{DCBS}}(R), \tag{1}$$

where E_{RgS} is the energy of the dimer, $E_{\mathrm{Rg}}^{\mathrm{DCBS}}$ and $E_{\mathrm{S}}^{\mathrm{DCBS}}$ are the energies of the monomers calculated with the dimer-centered basis set (DCBS) and R is the internuclear distance. The interaction energies are corrected for the basis set superposition error (BSSE) by using the counterpoise procedure of Boys and Bernardi.[36]

Calculations of the nonrelativistic potentials are performed with augmented correlation consistent quadrupole zeta basis sets aug-cc-pVQZ (hereafter, VQZ) augmented by the $[3s3p2d]$ set of the bond functions. The bond functions are centered at the midpoint between the sulfur atom and the rare gas atom and have the exponents sp: 0.9, 0.3, 0.1; d: 0.6, 0.2. The resulting basis set is denoted by VQZ+332. In the case of the XeS system, the relativistic effective core potential ECP46MWB for the Xe atom and the VQZ basis set for the S atom with the same 332 bond functions are employed.

The post-Hartree–Fock interaction energies are obtained at the unrestricted coupled cluster UCCSD(T) level of theory, based on the single reference RHF wave function, as described in Refs. 37 and 38. The resulting set of *ab initio* potentials is designated below by UCCSD(T)/VQZ+332 (UCCSD(T)/VQZ/ECP+332 for XeS). Only the valence shell is correlated. The internuclear distance R was varied in the range (1.25 Å, 12.0 Å) for HeS, (1.5 Å, 12.0 Å) for NeS, (1.75 Å, 12 Å) for ArS, (2.0 Å, 12.0 Å) for KrS, and (2.0 Å, 15.0 Å) for XeS. The spin contamination $\langle S^2-S_z^2-S_z\rangle$ is small ($\sim$0.002) for all complexes under consideration, it is the same as for the isolated S atom and does not change with the distance.

The most accurate scattering data are available for the NeS system.[32] Therefore, we present a more extensive *ab initio* analysis for this system. First, we use an extended aug-cc-pV5Z basis (V5Z) supplemented with a larger $[3s3p2d2f1g]$ set of bond functions with the exponents (sp: 0.9, 0.3, 0.1; df: 0.6, 0.2; g: 0.3). This basis set is denoted by V5Z+33221. Second, another version of the coupled cluster method is applied, including triples at the fourth order, UCCSD[T],[39,40] with the same V5Z+33221 basis set. Finally, the calculations which correlate all shells of Ne and S except for only the innermost 1s orbitals are performed. This calculations are referred to as UCCSD[T]/fc($1s$)/V5Z+33221.

The electronic structure calculations are performed with the MOLPRO2000 suite of programs.[40]

The *ab initio* points for both the $^3\Pi$ and $^3\Sigma^-$ states are fitted by the analytical expression of the Degli Esposti–Werner-type,[42] composed from the short-range term (V_{sh}) and the asymptotic long-range part (V_{as}),

$$V(R)=V_{\mathrm{sh}}(R)+V_{\mathrm{as}}(R), \tag{2}$$

where

$$V_{\mathrm{sh}}(R)=\sum_{l=0}^{8} g_l R^l e^{-\alpha(R-\beta)}. \tag{3}$$

The long-range part is represented by the damped dispersion term,

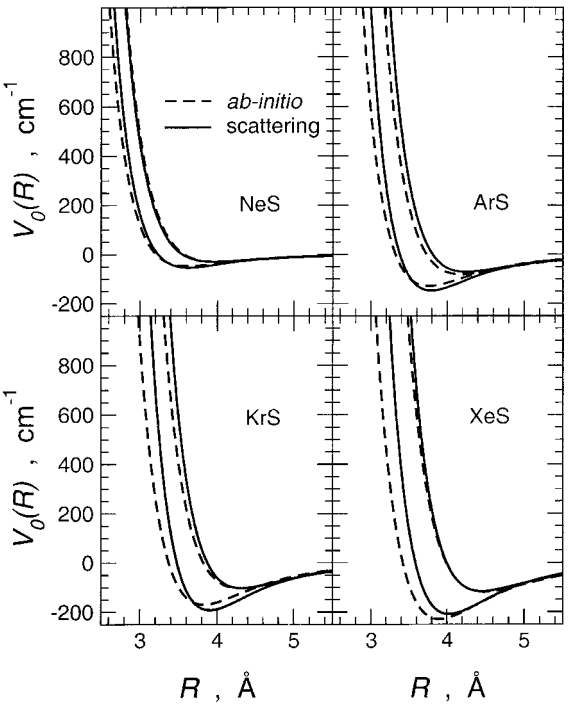

FIG. 1. Scattering and *ab initio* $V_\Sigma(R)$ and $V_\Pi(R)$ potentials for the NeS, ArS, KrS, and XeS dimers.

$$V_{\mathrm{as}}(R)=-\frac{1}{2}[1+\tanh(\gamma+\delta R)]\sum_{n=0}^{4}\frac{C_{2n+6}}{R^{2n+6}}. \tag{4}$$

The nonlinear α, β, γ, δ and the linear g_l and C_i parameters are optimized using the Levenberg–Marquardt least-square algorithm with no constraints imposed. It turns out that whereas the lower C_i coefficients ($i=6, 8, 10$) account essentially only for dispersion and induction van der Waals interaction, the C_{12} term contributes to repulsion [remember that the $1/R^{12}$ dependence has been efficiently employed to model repulsion in the classic Lennard-Jones (12-6) potential]. The maximum root-mean-square (RMS) error is 0.05 cm^{-1}, and the RMS error averaged over the internuclear distance does not exceed 0.03 cm^{-1}. The Fortran code that generates the potentials is available from the authors upon request, as well as the one generating the ''scattering'' potentials, to be encountered below.

B. The interaction potentials

The scattering and the *ab initio* V_Σ and V_Π potentials are shown in Fig. 1, while their zero points, equilibrium distances, and well depths are collected in Table I.

In general, the *ab initio* data for Rg from Ne to Xe fall within the error bars of the scattering experiments.[32] For all Rg atoms except Ar, the agreement is markedly better for the excited $^3\Sigma^-$ state than for the ground $^3\Pi$ state. The *ab initio* calculations for the ground state generally lead to shorter equilibrium distances and smaller interaction energies, with the exception of the XeS system. The *ab initio* potentials of the excited states also have slightly shorter R_e but their D_e values are in excellent agreement with experimental data except for the ArS system.

TABLE I. Zeros σ, Å, equilibrium distances R_e, Å, and well depths D_e, cm^{-1} for the scattering and *ab initio* potentials of the $^3\Pi$ and $^3\Sigma^-$ states of the Rg–S systems.

		Scattering		UCCSD(T)/VQZ+332	
System	Parameters	$^3\Pi$	$^3\Sigma^-$	$^3\Pi$	$^3\Sigma^-$
HeS	σ	⋯	⋯	3.244	3.739
				3.24[a]	3.73[a]
	R_e	⋯	⋯	3.653	4.188
				3.65[a]	3.18[a]
	D_e	⋯	⋯	19.94	10.60
				20.1[a]	10.7[a]
NeS	σ	3.23± 0.13	3.55± 0.14	3.223	3.589
				3.212[b]	3.580[b]
				3.206[c]	3.575[c]
				3.206[d]	3.575[d]
	R_e	3.62± 0.14	3.97± 0.16	3.625	4.024
				3.614[b]	4.013[b]
				3.608[c]	4.008[c]
				3.604[d]	4.003[d]
	D_e	53.2 ±13	29.0 ± 7	44.60	29.03
				46.17[b]	29.48[b]
				47.03[c]	29.97[c]
				47.55[d]	30.24[d]
ArS	σ	3.38± 0.10	3.81± 0.11	3.319	3.726
	R_e	3.79± 0.11	4.24± 0.13	3.755	4.186
	D_e	148.4 ±22	72.6 ±11	129.76	82.15
KrS	σ	3.48± 0.10	3.87± 0.12	3.373	3.822
	R_e	3.91± 0.12	4.32± 0.13	3.826	4.295
	D_e	192.0 ±29	103.2 ±15	169.49	103.01
XeS	σ	3.58± 0.11	4.00± 0.12	3.418	3.988
	R_e	4.02± 0.12	4.45± 0.13	3.897	4.482
	D_e	209.7 ±31	115.3 ±17	229.45	118.43

[a]UCCSD(T)/VQZ+33211 calculations from Ref. 35.
[b]UCCSD(T)/V5Z+33221 calculations.
[c]UCCSD[T]/V5Z+33221 calculations.
[d]UCCSD[T]/fc(1*s*)/V5Z+33221 calculations.

Extended calculations for NeS indicate that the UCCSD(T)/VQZ+332 calculations are not fully converged with respect to either the basis set size or the level of correlation treatment (although the convergence error is only of the order of 5%). Interestingly, all factors (the use of extended basis set, the implementation of the UCCSD[T] method, and the account for the correlation of inner shells) increase the binding energy in the $^3\Pi$ state improving the agreement with the scattering data. The same holds true for the $^3\Sigma^-$ state, but the net effect is much less significant. At the same time, the improvements of the *ab initio* calculations systematically shorten the equilibrium distances in both electronic state, increasing the deviation from the experimental results. The effect of the basis set size is most significant. The *ab initio* results of Partridge *et al.*[35] obtained at the UCCSD(T)/VQZ+33211 level of theory for HeS are also presented in Table I. They are in excellent correspondence with the present UCCSD(T)/VQZ+332 ones indicating that the augmentation of atom-centered part of the basis (from VQZ to V5Z) is presumably more important than the augmentation of the bond function set (from 332 to 33211).

It is also instructive to compare qualitative trends in the sequence of Rg atoms. According to our *ab initio* calculations, HeS is a distinct system with relatively large equilibrium distances R_e in both electronic states. Indeed, passing to Ne, one observes a significant reduction of equilibrium distance which then monotonically increases from Ar to Xe. The same trend is shown by the scattering potentials. The interaction anisotropy, taken as the difference between V_Π and V_Σ potentials, also increases from He to Xe.

Recent *ab initio* studies of Rg-open shell interactions by Burcl *et al.*[26] and by Buchachenko *et al.*[28] contributed to elucidate the nature of the Rg-atom potentials. The anisotropy of such interactions is related to different orientations of the open-shell moiety's singly- and doubly-occupied orbitals with respect to the Rg atom; we refer to them as the pair-electron contact and the single-electron contact. The pair electron contact results in the binding that is characteristic for the interaction of closed-shell species, such as that arising between two Rg atoms. The single-electron contact, however, reveals a substantially stronger attraction.

Ab initio calculations of RgCl (Refs. 26 and 27) and RgO, RgO^- interactions[28] by means of combined supermolecular and perturbation theory approaches provided direct and explicit evaluation of the fundamental components of the binding energy: induction, dispersion, and exchange-repulsion. In particular, they enabled to find out which of

these components determines especially strong stabilization of the single electron contact.

First, it should be noted that the long-range induction component (determined by the interaction of the quadrupole of open-shell moiety with the induced dipole at the Rg atom) is practically negligible. Although its relative anisotropy is large—asymptotically of the order of 70%—yet the induction effect decays as $1/R^8$ and as a whole is quantitatively negligible.

Second, only a small portion of the stronger binding may be attributed to a larger van der Waals attraction—a greater dispersion effect. The dispersion anisotropy may be approximately related to the anisotropy of the static dipole polarizability of the open-shell. Asymptotically, the effect decays as $1/R^6$ and the anisotropy is, for the RgCl and RgO dimers, of the order of 10% only.

The decisive factor is the anisotropy of the short-range repulsion, the component often referred to as the exchange-repulsion or Heiltler–London exchange. In the van der Waals minimum region, for the single-electron contact the exchange repulsion is reduced by a factor of 2 in comparison to a pair-electron contact in all complexes studied so far by the *ab initio* method, RgCl and RgO, RgO^-. The Heiltler–London exchange is due to such quantum mechanical features as delocalization of the electrons and their indistinguishability. It corresponds to ''resonance'' integrals in the Pauling description of chemical bonds and is related to the Pauli principle.

In the molecular orbital (MO) language in terms of occupation of bonding and antibonding orbitals, one may bring the example of the He_2 complex and of the He_2^+ molecule. He_2 is a model for a pair-electron contact, where the stabilizing effect of two electrons sitting on bonding orbitals is fully canceled by the destabilizing effect of a two electrons sitting on antibonding orbitals. In the He_2^+ molecule, a model of a single-electron contact, only half of the binding effect is cancelled. One may say that an incipient, single-electron, chemical bond is created.

The different nature of the $^3\Sigma^-$ and $^3\Pi$ states of RgS is demonstrated in Fig. 2, where reduced potentials for ArS $^3\Pi$ and $^3\Sigma^-$ states are plotted along with the V_0 isotropic part and the reduced potential of the Ar dimer from Ref. 18. The reduced potentials are derived by representing the potential curves $V(R)$ in the R_e and D_e units: $V(x)/D_e$ with $x = R/R_e$. According to the principle of corresponding states (see, e.g., Ref. 41) the reduced potentials should be identical, that is the interaction should be described by the same dimensionless universal function, when the nature of the interaction is the same. One can see that the V_Σ potential closely follows the Ar dimer potential, corroborating a similar nature of both. By way of contrast, in particular in the repulsive region [see Fig. 2(c)], the V_Π potential is distinctly different. It is worthwhile to note that all RgS V_Σ and all RgS V_Π potentials, if drawn in the same Fig. 2, would practically coincide with the ArS V_Σ potential and ArS V_Π potential, respectively.

An alternative formulation of the short-range electronic energy distribution has been recently set forth by Pirani *et al.* [24] who linked the enhanced binding of the Rg-open-shell

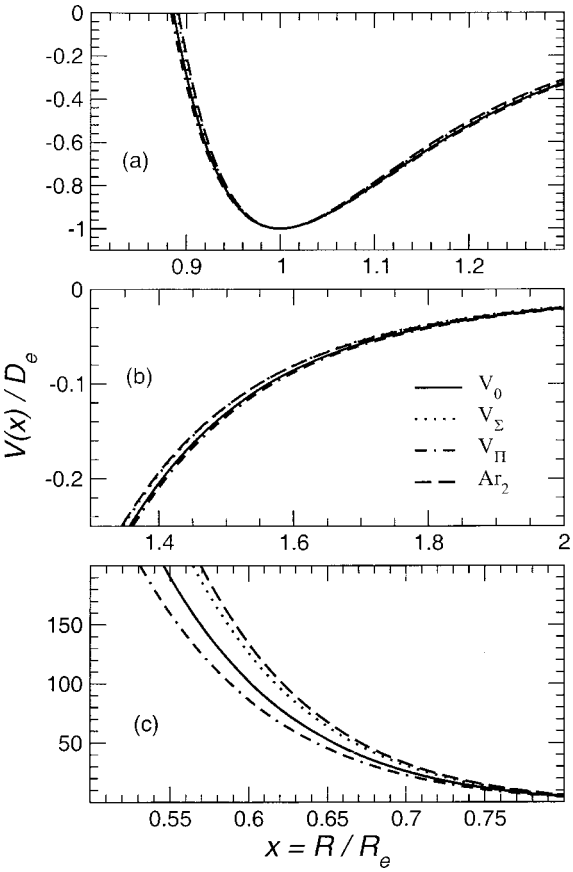

FIG. 2. Scaled curves for the $^3\Pi$, $^3\Sigma^-$, and V_0 potentials for the ArS system from the present work, compared with the potential curve of the Ar dimer (Ref. 18).

interaction with the nonresonant charge-transfer, and the coupling between diabatic covalent and ionic states. This model was proved to provide reasonable estimates of the anisotropy of the interaction at short range and will also be successfully used later in Sec. IV. The incipient bond is here attributed to the additional stabilization due to electron-transfer and to the resulting contribution from anion–cation interaction.

It should be stressed that both the MO approach of the *ab initio* calculations and the description in terms of covalent and ionic states originating from the valence bond (VB) theory are equivalent if the wave function expansion is elaborate enough, that is, if it is carried out beyond the HF level of theory within the MO framework, and includes a variety of covalent and ionic structures within the VB theory. The power of the molecular orbital method is its highly advanced computational technology. The usefulness of the valence bond approach is in its transparent relationship to the intuitive physical picture of the interaction, and the possibility of direct reference to monomer properties: polarizabilities, ionization potentials, electron affinities, etc., an indispensable prerequisite to establish empirical correlation relationships.[24]

C. Atomic model for the spin–orbit coupling

Spin–orbit interaction determines the mechanism of inelastic intramultiplet mixing, and is known to severely affect

the elastic scattering of open-shell atoms. The standard way to take it into account[43] is to introduce an approximate spin–orbit Hamiltonian with only the contribution from the isolated atom,

$$\hat{H}_{\mathrm{SO}} = a\hat{L}\hat{S}, \tag{5}$$

where $\hat{L}$ and $\hat{S}$ are the orbital and spin electronic angular momenta of the openshell atom, respectively. The spin–orbit constant a is related to the spin–orbit splittings of the atomic level Δ_j, so that the energies of excited atomic sublevels $j=1$ and $j=0$ with respect to the ground $j=2$ sublevel are $\Delta_1 = 2a$, $\Delta_0 = 3a$. The matrix elements of the spin–orbit Hamiltonian (5) can be easily obtained using the atomic electronic functions in the Hund case (a) representation. The diagonalization of the total (electrostatic plus spin–orbit) Hamiltonian matrix gives a set of six relativistic adiabatic potentials, while its transformation to the Hund case (c) basis gives the relativistic Hamiltonian matrix in the diabatic representation which is suitable for studying inelastic collisions. The analytical expressions for Hamiltonian matrices in the diabatic and adiabatic representations in terms of V_Σ, V_Π, and atomic spin–orbit splittings Δ_j relevant to the Rg–S(^3P_j) systems can be found in Refs. 28, 29, 44–47.

The deviation from the atomic model may occur in the short-range interaction region due to mixing with upper electronic states or due to the failure of the approximation (5). In order to verify the validity of the atomic model, direct calculations of the spin–orbit coupling matrix elements between the $^3\Pi$ and $^3\Sigma^-$ states of the NeS and XeS have been performed using the method of diagonalization of the $\hat{H}_{\mathrm{el}} + \hat{H}_{\mathrm{SO}}$ operator[48] which is implemented in the MOLRPO2000 suite of programs.[40] The Ne and S atoms are described using the uncontracted VQZ basis set, while for the Xe atom we adopt the pseudopotential Stuttgart ECP46MWB($spdf$) basis set. The complete Breit–Pauli spin–orbit Hamiltonian ($\hat{H}_{\mathrm{SO}}$) is expressed in the basis of adiabatic states of the $\hat{H}_{\mathrm{el}}$ Hamiltonian. In the case of NeS, only two states correlating with the ^3P state of the sulfur atom are included in the diagonalization procedure. For the XeS system, this basis set is also augmented by the states correlating to the ^1S and ^1D states of the sulfur atom.

Asymptotic values of the spin–orbit coupling matrix element are equal to 193.1 and 194.5 cm^{-1} for the minimum and extended bases of the adiabatic states, respectively. The corresponding splittings are $\Delta_1 = 386.2$, $\Delta_0 = 579.3\,\mathrm{cm}^{-1}$, and $\Delta_1 = 389.0$, $\Delta_0 = 583.5\,\mathrm{cm}^{-1}$, respectively. The effect of coupling with the states correlating to excited atomic limits is small, but brings the atomic splittings to better agreement with experimental data [$\Delta_1 = 396.2$, $\Delta_0 = 573.4\,\mathrm{cm}^{-1}$ (Ref. 49)]. The calculated spin–orbit matrix elements are plotted in Fig. 3.

The matrix elements are almost independent of the interatomic separation down to relatively short internuclear distances and then show a rapid decrease. For NeS, this decay occurs at a rather small distance, well outside the region of importance for collision dynamics. However, for XeS the short-range deviation from the atomic model starts in the neighborhood of R values corresponding to the zero of the $^3\Pi$ potential. The test calculations performed with the *ab initio* R-dependent couplings demonstrate that this does not effect significantly the results of the scattering calculations discussed below. However, it should be noted that such a deviation from atomic approximation can be quite important for high-energy collisions, which probe the repulsive part of the interactions.

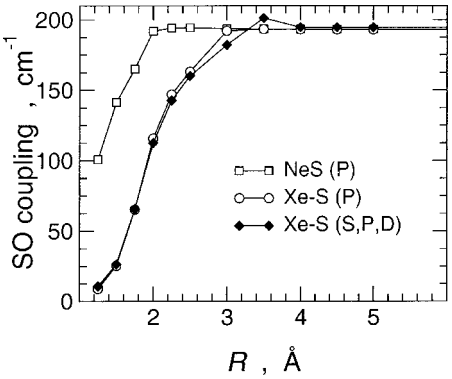

FIG. 3. Spin–orbit matrix elements in the NeS (VQZ basis) and XeS [ECP46MWB+$spdf$(VQZ) basis] systems as a function of the internuclear distance.

III. ANALYSIS OF TOTAL SCATTERING CROSS SECTIONS

A. Methods of calculation

The theory needed to interpret the experimental scattering results and obtain information on the involved interaction potentials has been described[44,45,50] and reviewed[2] elsewhere. Therefore only the aspects relevant to present purposes will be summarized below.

For the analysis of scattering experiments it is most natural to represent the interaction between a P-state atom (such as sulfur in its ground state) and a ^1S rare gas atom in terms of two R-dependent functions, the spherical $V_0(R)$ and anisotropic $V_2(R)$ components of the electrostatic potential. They are related to the more familiar $V_\Sigma(R)$ and $V_\Pi(R)$ potential curves considered in the previous section by[44,45,51]

$$V_0 = \frac{V_\Sigma + 2V_\Pi}{3}; \quad V_2 = \tfrac{5}{3}(V_\Sigma - V_\Pi), \tag{6}$$

or inversely,

$$V_\Sigma = V_0 + \tfrac{2}{5}V_2; \quad V_\Pi = V_0 - \tfrac{1}{5}V_2. \tag{7}$$

The usefulness of this representation derives from separation of the interaction energy into an isotropic and an anisotropic components, V_0 and V_2, respectively.

To calculate, from given V_0 and V_2, absolute total scattering cross sections (ATCS) we use the same approach which was implemented for the analysis of molecular beam measurements in Ref. 32.

In the low collision energy range, the scattering involves only the manifold of electronic states correlating with the ground atomic levels ^3P_j of the open-shell sulfur atom, and therefore only the fine-structure components and the centrifugal potential couplings are added to provide full potential energies in a multichannel Schrödinger equation. For a sufficiently high spin–orbit splitting, as in the case of sulfur,

the centrifugal component in the potential energy matrix essentially reduces to a diagonal term [Hund's cases (c), at long-range, and (a), at short-range[2,44,45]] and collisions can be considered to take place along six relativistic adiabatic potentials $V_{j,\Omega}$ (Ω being the projection of j along the internuclear axis). These terms are obtained by diagonalization of the potential energy matrix which includes electrostatic and atomic spin–orbit components but neglects centrifugal couplings. The curves $V_{j,\Omega}$ are represented by a proper combination of V_0, V_2 and fine structure component terms.[32]

ATCS for each potential $V_{j,\Omega}$ are calculated using the semiclassical[53] and exact quantum approaches as a function of the center-of-mass velocity. We have found that both methods led to essentially the same results and thus in the following we present only the semiclassical calculations.

The measured cross section $Q(v)$, in the adiabatic representation, is given as a weighted sum of cross sections for scattering by each of the adiabatic potentials. In these experiments, the sublevels of sulfur atoms have been assumed to be populated according to their degeneracies.[32] After the summation, the total ATCS is transformed to the laboratory frame to account for spreading of the laboratory velocity of the sulfur beam and the thermal motion of the rare gas target.

The long-range part of the V_0 component of the interaction is directly probed in the experiments, because of the accurate calibration of the absolute value of the cross sections (within an uncertainty on the leading long-range coefficient of about 7%). Indeed, the absolute value of the elastic cross section is determined mainly by the C_6 coefficient and only to a minor extent by higher order terms, whose effect is attenuated in the distance range probed by the experiment. Accordingly, the analysis of the experimental data[32] has been made in term of an ''effective'' long-range coefficient which includes also the higher order contributions and therefore is expected to exceed the calculated C_6 coefficient by $\sim$20%.[23] The experimental effective long-range coefficients refer to the spherical interaction, the absolute value of the cross section being uneffected by the anisotropy. Therefore, it is possible to compare the calculated *ab initio* long range part of the S–Rg interaction with the experimental cross section data, by fitting the behavior of the calculated potentials, in the long range, with a flexible functional form including contributions from terms of higher order than C_6. In this way it has been possible to improve the calculated cross sections, including the C_8 contribution, with the use of the Fontana–Bernstein model[54] and to make a direct comparison with the experiments. The results are very satisfactory for the NeS and ArS cases, while for KrS and XeS they suggest that the long range average attraction in the *ab initio* calculations is overestimated by $\sim$10%.

B. Comparison with experimental data

The ATCS calculated using the *ab initio* potentials for the NeS system are reported in Fig. 4 together with experimental data, as a function of the sulfur beam velocity. Figure 5 illustrates the cases of ArS, KrS, and XeS collisions. In the same figures the results using the scattering potentials (solid lines) obtained by a direct best-fit analysis of the experiments[32] are also reported.

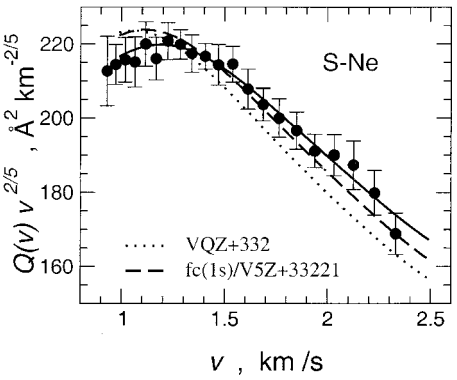

FIG. 4. Experimental absolute total cross sections for the S(^3P_j)–Ne system. Calculated cross section using a best fit *scattering* potentials (solid line) and the *ab initio* potentials evaluated with different basis sets are also reported.

The overall performance of the *ab initio* potentials is very good; for all systems, they reproduce both the magnitude and the qualitative structure of glory undulations. However, there are some quantitative differences. They deserve a special discussion in order to shed light not only on the quality of the *ab initio* calculations but also on the sensitivity of the scattering cross sections to specific features of the interaction potentials.

The experimental data for the NeS case characterize mainly $V_0(R)$, the isotropic part of the interaction.[32] The *ab initio* potentials underestimate ATCS at high energies and do not reproduce the position of the glory maximum. This is due to the underestimation of the ''area'' of the well of the V_0 component of the interaction (roughly the well depth times the well location). In the case of the less advanced calcula-

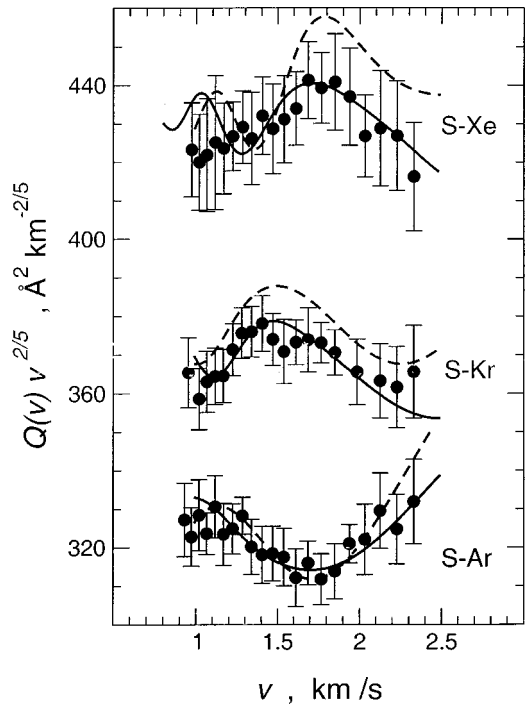

FIG. 5. Experimental absolute total cross sections for the S(^3P_j)–Ar, Kr, and Xe systems. Calculated cross section using a best fit *scattering* potentials (solid line) and the *ab initio* potentials are also reported.

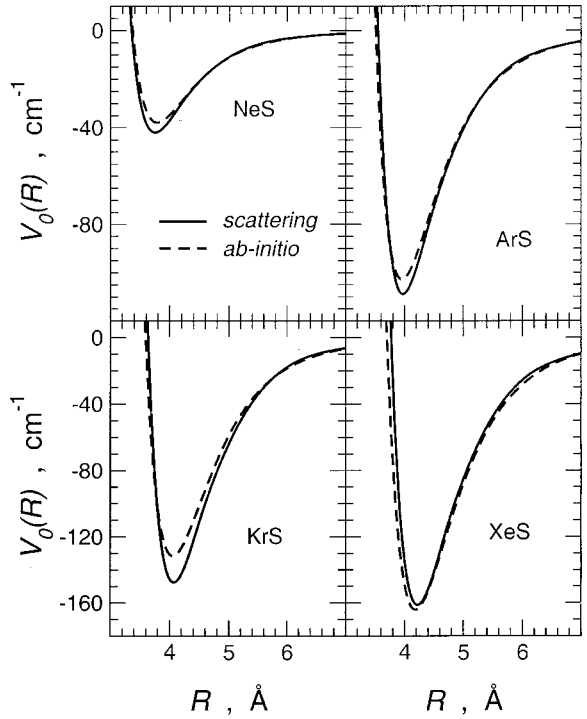

FIG. 6. Scattering and *ab initio* $V_0(R)$ potentials for the NeS, ArS, KrS, and XeS dimers.

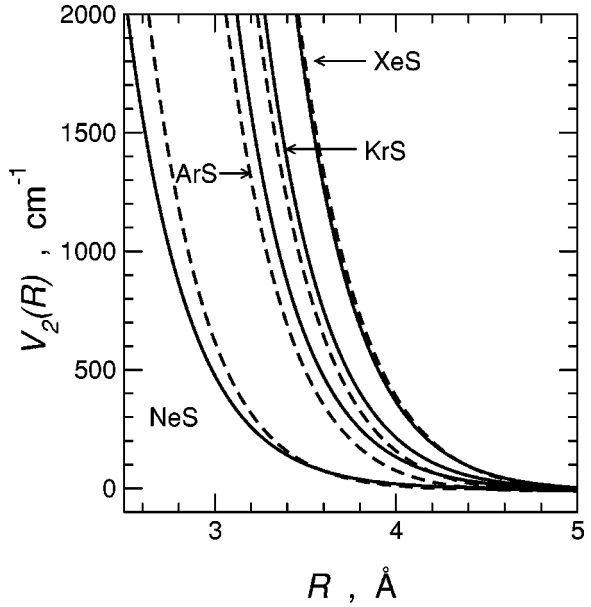

FIG. 7. Scattering and *ab initio* $V_2(R)$ potentials for the NeS, ArS, KrS, and XeS dimers.

tions the underestimation of the well area is of the order of 15%. However, it follows from Fig. 4 that more extensive *ab initio* calculations give a larger well area and a better agreement with experimental data.

The glory pattern is reproduced quite well for the ArS and KrS systems, despite the overestimation of the ATCS in the latter case. This is an indication that for KrS the *ab initio* calculations overestimate the long range attraction.

For XeS, the performance of the *ab initio* potentials is less impressive (but still acceptable in view of the system size and the large uncertainty of the measured data). The predicted frequency of glory oscillations is too high and their amplitude is too large. This is probably due to the overestimation of the well depth of the $^3\Pi$ potential or, in other words, to the overestimation of the anisotropic V_2 component of the interaction.

IV. COMPARISON OF *AB INITIO* AND SCATTERING POTENTIALS

The V_0 and V_2 potentials obtained from the best fit to the experimental data and by combining the *ab initio* V_Π and V_Σ potentials with Eq. (5) are compared in Figs. 6 and 7, which show an overall satisfactory agreement. Table II reports the main characteristics of the V_0 and V_2 interaction potentials. Features such as well depths D_e and their locations R_e (see Table II) are seen to regularly increase from NeS to XeS, confirming general trends previously observed for the interactions of O,[6] F,[7] and Cl (Ref. 8) with rare gases. A comprehensive analysis[23] of the large amount of data presently available for the $V_0(R)$ interaction, for a variety of systems, consistent[52] with the concept of corresponding states already encountered in Sec. II B, have allowed us to characterize the nature of this component, in the neighborhood of the potential minimum and at long intermolecular distances, as basically due to forces typical of van der Waals interactions. The agreement shown in Table II for D_e and R_e parameters obtained by the *ab initio* and scattering V_0 potentials and those calculated from formulas in Ref. 23 can be taken as a further strong evidence that the spherical V_0 interaction term, at intermolecular distances comparable with R_e or larger, shows the features of a typical van der Waals potential, for which the empirical correlation formulas[23] have been developed and verified.

The observed trend in the V_2 anisotropic term (Fig. 7) also indicates that its role increases from He to Xe. The increase in the differences between V_Π and V_Σ potentials cannot be explained on the basis of the interaction anisotropy of the van der Waals-type, as already discussed in Sec. II B. Table II reports the values of the V_2 term at the distance $R=\sigma$, where the V_0 term is zero. The choice of this particular reference distance is motivated by a recent analysis of the correlation between bond stabilization in open-shell systems and the parameters describing charge transfer effects.[24] Relevant information on this interaction was obtained by the analysis of bond stabilization in halides, oxides, sulfides, and ionic dimers of rare gases. Most of this information comes from recent molecular beam experiments and leads to the characterization of the dependence of the charge-transfer matrix element on basic physical properties of the interacting partners. The magnitude of the coupling matrix element was correlated to properties of the individual interacting partners such as polarizabilities, charges, electron affinities, and ionization potentials. We include in Table II the results of Ref. 24. As already anticipated in Sec. II B, being based on the valence bond theory, this approach gives an intuitive physical picture of the interaction and suggests that the stabilizing contribution to the bond depends on the energy separation between ionic and covalent states; its observed increase from

TABLE II. Zeros σ, Å, equilibrium distances R_e, Å, and well depths D_e, cm^{-1} of the spherical component of the interaction V_0. The value of the V_2 at σ of V_0 is also reported, in cm^{-1}.

System		UCCSD(T)/VQZ+332	Scattering	Correlation formulas
HeS	σ	3.48		
	R_e	3.91		3.74[a]
	D_e	14.3		20[a]
	$V_2(\sigma)$	86		44[b]
	$V_2(\sigma)/D_e$	6.0		2.2
NeS	σ	3.39	3.35	
	R_e	3.77	3.75	3.77[a]
	D_e	36	42	42[a]
	$V_2(\sigma)$	164	164	110[b]
	$V_2(\sigma)/D_e$	4.6	3.9	2.6
ArS	σ	3.51	3.55	
	R_e	3.95	3.97	3.97[a]
	D_e	103	109	102[a]
	$V_2(\sigma)$	476	549	423[b]
	$V_2(\sigma)/D_e$	4.6	5.4	4.2
KrS	σ	3.58	3.64	
	R_e	4.05	4.07	4.07[a]
	D_e	132	148	148[a]
	$V_2(\sigma)$	661	661	740[b]
	$V_2(\sigma)/D_e$	5.0	4.5	5.0
XeS	σ	3.70	3.78	
	R_e	4.18	4.20	4.22[a]
	D_e	165	161	156[a]
	$V_2(\sigma)$	992	729	984[b]
	$V_2(\sigma)/D_e$	6.0	4.5	6.3

[a]Reference 23.
[b]Reference 24.

He to Xe can indeed be correlated with the decreasing ionization potential of the rare gas partners. Interestingly, while for the heavier rare gases the various methods give results in a qualitative good agreement, for NeS the agreement is not satisfactory, and for HeS a difference by a factor of 2 is found between the *ab initio* and the correlation formula values. This may be an indication that chemical stabilization and polarization anisotropy effects play a comparable role in the HeS systems since the empirical correlation formulas neglect any contribution coming from the anisotropy of polarizability of the sulfur atom (responsible for the anisotropy of the van der Waals interaction component). This is reasonable since for He one can expect the largest relative van der Waals anisotropy because of the smallest ''size'' of the the atom, which has not only the smallest polarizability but also the highest ionization potential (and thus the smallest chemical stabilization by electron transfer). To some extent a similar argument also pertains to Ne, for which some disagreement is observed, too.

It is also interesting to determine how the potential component V_2 derived from different sources deviates from the principle of corresponding states.[41] Following this principle, in the ideal case, the ratio of $V_2(\sigma)$ and D_e should be constant for different rare gases. These ratios are given in Table II. One can see that both *ab initio* and scattering results provide fairly consistent values of $V_2(\sigma)$. The correlation formulas work also well except for He and Ne, in accord with the above discussion.

V. INTRAMULTIPLET TRANSITIONS IN Rg+S COLLISIONS

Despite the lack of experimental data, the investigation of the collision-induced transitions between the $j=0$, 1, and 2 levels of the ^3P_j multiplet in sulfur atoms are of both methodological and practical interest. Inelastic transitions in the $Rg+X(^3P)$ collisions have been studied in several works, see, e.g., Refs. 29, 30, 44–47, 55. It is well known that the electrostatic interaction which preserves the body-fixed projection Ω of $\mathbf{j}$ (and simultaneously of the total angular momentum $\mathbf{J}$) couples the $j=0$, 2 and $j=1$, 2 pairs of levels. The corresponding transitions are therefore allowed in the zero-order approximation. The third $j=0\rightarrow j=1$ transition is often termed as ''forbidden,'' because the direct coupling between these levels vanishes. This transition is assisted by Coriolis interaction which couples the Ω components within the same j manifold. Recently, we have shown that the forbidden transition proceeds through a complicated postcollision relaxation involving sequential transitions induced by both electrostatic and Coriolis couplings.[29] It is of interest to analyze the trends in the intramultiplet mixing rates when passing from oxygen to the heavier sulfur atom. In addition, the rate constants calculated here for the first time may be useful for kinetic models of energy transfer and reactions involving sulfur atoms.

The calculations are performed using rigorous quantum mechanical close coupling (CC) technique[56,57] as described elsewhere.[29,30] The model with a constant spin–orbit coupling parameterized by experimental values of the splitting between the sublevels of the S atom (Sec. II C) is implemented, except for test calculations for Xe+S collisions where the *ab initio* R-dependent spin–orbit couplings are used. The inelastic cross sections for all three relaxation transitions are calculated on an energy grid of more than 100 points and the corresponding rate constants in the temperature range 20–2000 K are obtained by numerical integration. The rate constant values are converged to within 1% at $T=100-1500$ K and 5% at higher temperatures. The low-energy collisions are affected by numerous shape resonances so a finer energy grid is implemented to evaluate the rate constants at $T<100$ K with an accuracy better than 20%.

Table III lists the rate constants for spin–orbit relaxation at room temperature in Rg+S collisions in comparison with the data on the Rg+O collisions[30] calculated for the scattering[6] and *ab initio* potentials, which were obtained using similar procedures as the RgS potentials discussed here. For brevity of the presentation we do not include rate constants at other temperatures in this article, but they may be obtained upon request from the authors.

The rate constants for Rg+S collisions calculated on the scattering and *ab initio* potentials agree well with each other. The ratio of the rate constants obtained on the different potentials does not exceed a factor of 2 in the worst case. The cross sections for two allowed transitions in Ne+S collisions calculated on two different *ab initio* potentials are in excellent agreement with each other. The deviation between the

TABLE III. Room-temperature rate constants (cm^3/s) for intramultiplet $j \rightarrow j'$ transitions in collisions of $S(^3P)$ and $O(^3P)$ with rare gas atoms computed with two different sets of interaction potentials. Numbers in parentheses indicate the power of 10. The data for O+Rg are taken from Ref. 30.

		Rg+S			Rg+O		
Rg	Potentials	0→2	1→2	0→1	0→2	1→2	0→1
He	Scattering	⋯	⋯	⋯	1.52(−10)	1.02(−10)	4.77(−12)
	Ab initio	2.73(−12)	5.11(−12)	8.17(−13)	1.34(−10)	8.38(−11)	9.09(−12)
Ne	Scattering	9.55(−14)	2.15(−13)	8.78(−14)	2.95(−11)	1.72(−11)	2.24(−12)
	Ab initio	2.64(−13)	1.86(−13)	1.79(−13)	2.13(−11)	2.41(−11)	3.22(−12)
	Ab initio[a]	2.69(−13)	1.86(−13)	2.15(−13)	⋯	⋯	⋯
Ar	Scattering	1.27(−13)	7.76(−14)	3.94(−13)	1.81(−11)	1.87(−11)	3.33(−12)
	Ab initio	1.46(−13)	1.24(−13)	3.49(−13)	8.50(−12)	7.56(−12)	5.69(−12)
Kr	Scattering	4.65(−14)	4.05(−14)	3.72(−13)	1.32(−11)	9.97(−12)	4.87(−12)
	Ab initio	6.21(−14)	5.32(−14)	4.06(−13)	2.31(−11)	2.01(−11)	4.28(−12)
Xe	Scattering	4.38(−14)	3.02(−14)	4.06(−13)	1.39(−11)	1.41(−11)	6.62(−12)
	Ab initio	4.49(−14)	3.40(−14)	6.89(−13)	⋯	⋯	⋯
	Ab initio[b]	3.87(−14)	3.90(−14)	5.94(−13)	⋯	⋯	⋯

[a]UCCSD[T]/fc(1*s*)/V5Z+33221 calculations.
[b]Calculated using *R*-dependent *ab initio* spin–orbit coupling matrix elements.

values calculated with the two potentials does not exceed 5%. The rate constant for the forbidden transition computed on the most accurate *ab initio* potential is larger than the rate constant computed on the "standard" UCCSD(T)/VQZ+332 potential by about 15%.

For Xe+S, the rate constants calculated on the *ab initio* potentials with *R*-dependent spin–orbit couplings are also presented. They differ from those obtained with the constant atomic spin–orbit couplings by 20%, but more than half of the difference is due to the deviation of the *ab initio* results for the asymptotic couplings from the experimental ones which introduces the difference in the energies of the *j* scattering channels.

The collisions with helium atoms are most efficient in inducing inelastic transitions. The efficiency of the allowed $j=0\rightarrow j=2$ and $j=1\rightarrow j=2$ transitions is reduced by an order of magnitude for neon and decreases slightly in the sequence from Ar to Xe. The rate of the forbidden $j=0\rightarrow j=1$ transition is less sensitive to nature of the collision partner, having the maximum value for He and the minimum value for Ne. All these trends are similar to those observed for the Rg+O collisions.[30]

The rate constants of allowed Rg+S transitions are on the average two orders of magnitude smaller than those for the transitions in Rg+O collisions, this being mainly due to the larger spin–orbit splittings (the spin–orbit splittings in oxygen atom are $\Delta_1=158.1\,cm^{-1}$ and $\Delta_0=226.6\,cm^{-1}$,[58] that is ≈2.5 times smaller than in sulfur, see above). However, the rate constant of the forbidden transition is smaller only by one order of magnitude. As a result, the $j=0\rightarrow j=1$ transition is relatively more efficient for sulfur than for oxygen. Indeed, for collisions with Rg=Ar–Xe, the transition to the $j=1$ level is a prominent relaxation pathway of $S(^3P_0)$ already at room temperature whereas for oxygen the forbidden transition starts to dominate only in the low temperature limit.[30]

According to the time-dependent analysis of the Rg+O inelastic collision dynamics,[29] the first step in the relaxation of $O(^3P_0)$ is the transition to the $j=2$ level which is due to the electrostatic coupling in the Hamiltonian matrix. Postcollision relaxation during the separation of the collision partners is assisted by the Coriolis coupling which couples the $\Omega=0$ component of the $j=2$ manifold to the $\Omega=\pm1$ components. The latter can relax to the $j=1$ level because of the electrostatic coupling. However, the efficiency of the two transitions induced by electrostatic couplings is two orders of magnitude smaller in sulfur than in oxygen. This means that the Coriolis coupling should be at least an order of magnitude more efficient in sulfur than in oxygen in order to compensate for the difference in the rate of the forbidden transition, despite the unfavorable mass ratio. Figure 8, which compares the state-resolved opacity functions for Xe

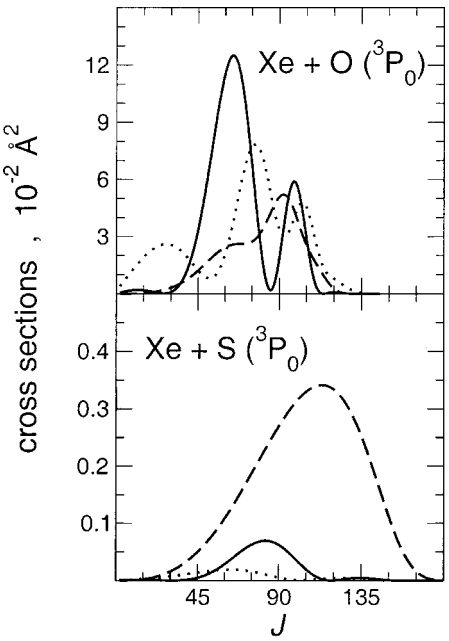

FIG. 8. Partial wave cross sections for spin–orbit relaxation in oxygen and sulfur atoms induced by collisions with Xe atoms at a collision energy of 1000 cm^{-1}. Solid curves, $j=0\rightarrow j=2$ transition; dashed curves, $j=0\rightarrow j=1$ transition; dotted curves, $j=1\rightarrow j=2$ transition.

$+O(^3P_0)$ and $Xe+S(^3P_0)$ collisions, provides an explanation. In the former case, the initial $j=0$, $\Omega=0 \rightarrow j=2$, $\Omega=0$ transition takes place efficiently at low values of the total angular momentum J, where the Coriolis coupling between the components of the $j=2$ manifold is not large. For the heavier Xe+S system with stronger interaction, more partial waves contribute to the scattering processes and the initial transition starts at higher J values. The Coriolis coupling which scales as J becomes more efficient in the postcollision relaxation. Interestingly, the difference of the interaction strengths in the Rg+S and Rg+O systems effects the transitions induced by the Coriolis couplings more *strongly* than the transitions induced by electrostatic couplings.

VI. CONCLUSIONS

The *ab initio* calculations of the Rg–S interaction potentials in the $^3\Pi$ and $^3\Sigma$-states are performed at the UCCSD(T) level of theory with an extended basis set (aug-cc-pVQZ augmented with bond functions). The results of the calculations are fit to flexible analytical forms and compared with *scattering* potentials, obtained by recent experimental studies.[32] The convergence of the *ab initio* calculations is tested for the NeS system. The saturation of the basis set, a more accurate account for the triple excitation (within the UCCSD[T] methodology), and the excitations from the core orbitals all act in the same direction, increasing the binding energy and reducing the equilibrium distance for both electronic states. The first factor is found to be most important. These results indicate that the convergence error of the present *ab initio* calculations does not exceed 10%.

Ab initio calculations of the spin–orbit coupling matrix element between the $^3\Pi$, $^3\Sigma^-$ states of NeS and XeS show that the coupling remains constant and equal to the atomic component down to relatively short internuclear distances. The deviation from the atomic spin–orbit coupling does not effect significantly the scattering dynamics at thermal energies.

A stringent test of the *ab initio* potentials is provided by comparison with the experimental data of the integral elastic cross sections calculated using these potentials in the laboratory frame. The overall performance of the *ab initio* potentials is very satisfactory; the quantitative small differences are discussed in order to delineate the quality of the *ab initio* calculations, and to elucidate the sensitivity of the scattering cross sections to specific features of the interaction potentials.

Cross sections and rate constants for inelastic intramultiplet transitions in the $S(^3P_j)+Rg$ collisions are computed using close-coupling technique. The reasonable agreement of the results obtained with *ab initio* and scattering potentials indicates the reliability of theoretical estimations for rate constants. It is shown that in contrast to O+Rg collisions, the ''forbidden'' Coriolis-assisted $j=0 \rightarrow j=1$ transition has a relatively large probability due to contribution from the scattering partial waves with high angular momentum, for which Coriolis coupling is very efficient.

ACKNOWLEDGMENTS

J.K. and G.C. are grateful to Professor Lucjan Piela for his comments on the rule of corresponding states. International collaboration is supported by NATO under linkage Grant No. CRG.LC 974215 by INTAS under Project No. 97-31573 and by the EU through the Human Potential Research Networks ''Generation, Stability, and Reaction Dynamics of Multiply Charged Ions in the Gas Phase'' (Contract No. HPRN-CT-2000-00027) and ''Theoretical Studies of Electronic and Dynamical Processes in Molecules and Clusters'' (Contract No. HPRN-CT-1999-00005). The contributions from the national foundations are also acknowledged: Russian Fund of Fundamental Research, Project No. 00-15-97346 by A.A.B.; Swedish Research Council by R.K.; the Polish Committee for Scientific Research KBN Grant No. 3 T09A 112 18 by J.K. and G.C.; National Science Foundation Grant No. CHE-0078533 by J.K. and G.C.; the Italian MIUR (Ministero dell'Istruzione, dell 'Università e della Ricerca), the ENEA (Ente per le Nuove Tecnologie, l'Energia e l'Ambiente) and ASI (Agenzia Spaziale Italiana) by V.A., F.P., and D.C.

[1] R. Candori, F. Pirani, and F. Vecchiocattivi, J. Chem. Phys. **84**, 4833 (1986).
[2] V. Aquilanti, G. Liuti, F. Pirani, and F. Vecchiocattivi, J. Chem. Soc., Faraday Trans. 2 **85**, 955 (1989).
[3] P. Casavecchia, G. He, R. K. Sparks, and Y. T. Lee, J. Chem. Phys. **75**, 710 (1981).
[4] P. Casavecchia, G. He, R. K. Sparks, and Y. T. Lee, J. Chem. Phys. **77**, 1878 (1982).
[5] V. Aquilanti, R. Candori, D. Cappelletti, V. Lorent, and F. Pirani, Chem. Phys. Lett. **192**, 145 (1992).
[6] V. Aquilanti, R. Candori, and F. Pirani, J. Chem. Phys. **89**, 6157 (1988).
[7] V. Aquilanti, E. Luzzatti, F. Pirani, and G. G. Volpi, J. Chem. Phys. **89**, 6165 (1988).
[8] V. Aquilanti, R. Candori, D. Cappelletti, E. Luzzatti, and F. Pirani, Chem. Phys. **145**, 293 (1990).
[9] V. Aquilanti, D. Cappelletti, V. Lorent, and F. Pirani, J. Phys. Chem. **97**, 2063 (1993).
[10] M. F. Golde and B. A. Thrush, Chem. Phys. Lett. **29**, 486 (1974).
[11] P. C. Tellinghuisen, J. Tellinghuisen, J. A. Coxon, J. E. Velasco, and D. W. Setser, J. Chem. Phys. **68**, 5187 (1978).
[12] G. Lo and D. W. Setser, J. Chem. Phys. **100**, 5432 (1994).
[13] A. Carrington, C. A. Leach, A. J. Marr, A. M. Shaw, M. R. Viant, J. M. Hutson, and M. M. Law, J. Chem. Phys. **102**, 2379 (1995).
[14] Y. Zhao, I. Yourshaw, G. Reiser, C. C. Arnold, and D. M. Neumark, J. Chem. Phys. **101**, 6538 (1994).
[15] I. Yourshaw, T. Lenzer, G. Reiser, and D. M. Neumark, J. Chem. Phys. **109**, 5247 (1998).
[16] T. Lenzer, I. Yourshaw, M. R. Furlanetto, G. Reiser, and D. M. Neumark, J. Chem. Phys. **110**, 9578 (1999).
[17] J. M. Hutson, A. Ernesti, M. M. Law, C. F. Roche, and R. J. Wheatley, J. Chem. Phys. **105**, 9130 (1996); Mol. Phys. **93**, 485 (1998).
[18] R. A. Aziz, in *Inert Gases*, edited by M. L. Krein (Springer, New York, 1984).
[19] V. Aquilanti, D. Cappelletti, V. Lorent, E. Luzzatti, and F. Pirani, Chem. Phys. Lett. **192**, 153 (1992).
[20] K. T. Tang and J. P. Toennies, J. Chem. Phys. **66**, 1496 (1977).
[21] R. Ahlrichs, R. Penco, and G. Scoles, Chem. Phys. **19**, 119 (1977).
[22] K. C. Ng, W. J. Meath, and A. R. Allnatt, Chem. Phys. **32**, 175 (1978).
[23] R. Cambi, D. Cappelletti, G. Liuti, and F. Pirani, J. Chem. Phys. **95**, 1852 (1991); D. Cappelletti, F. Pirani, and G. Liuti, Chem. Phys. Lett. **183**, 297 (1991); V. Aquilanti, D. Cappelletti, and F. Pirani, Chem. Phys. **209**, 299 (1996).
[24] V. Aquilanti, D. Cappelletti, and F. Pirani, Chem. Phys. Lett. **271**, 216 (1997); J. Chem. Phys. **106**, 5043 (1997); F. Pirani, A. Giulivi, D. Cappelletti, and V. Aquilanti, Mol. Phys. **98**, 1749 (2000).
[25] G. Chałasiński and M. M. Szczęśniak, Chem. Rev. **100**, 4227 (2000).

[26] R. Burcl, R. V. Krems, A. A. Buchachenko, M. M. Szczęśniak, G. Chałasiński, and S. M. Cybulski, J. Chem. Phys. **109**, 2144 (1998).
[27] A. A. Buchachenko, R. V. Krems, M. M. Szczęśniak, Y.-D. Xiao, L. A. Viehland, and G. Chałasiński, J. Chem. Phys. **114**, 9919 (2001).
[28] A. A. Buchachenko, J. Jakowski, G. Chałasiński, M. M. Szczęśniak, and S. M. Cybulski, J. Chem. Phys. **112**, 5852 (2000).
[29] R. V. Krems and A. A. Buchachenko, J. Phys. B **33**, 4551 (2000).
[30] R. V. Krems, A. A. Buchachenko, M. M. Szczęśniak, J. Kłos, and G. Chałasiński, J. Chem. Phys. **116**, 1457 (2002).
[31] A. A. Buchachenko, M. M. Szczęśniak, and G. Chałasiński, J. Chem. Phys. **114**, 9929 (2001).
[32] V. Aquilanti, D. Ascenzi, E. Braca, D. Cappelletti, and F. Pirani, Phys. Chem. Chem. Phys. **2**, 4081 (2000).
[33] A. V. Nemukhin, B. L. Grigorenko, and A. A. Granovsky, Chem. Phys. Lett. **301**, 287 (1999).
[34] M. Yamanishi, K. Hirao, and K. Yamashita, J. Chem. Phys. **108**, 1514 (1998).
[35] H. Partridge, J. R. Stallcop, and E. Levine, J. Chem. Phys. **115**, 6471 (2001).
[36] S. F. Boys and F. Bernardi, Mol. Phys. **19**, 553 (1970).
[37] P. J. Knowles, C. Hampel, and H.-J. Werner, J. Chem. Phys. **99**, 5219 (1999).
[38] P. J. Knowles, C. Hempel, and H.-J. Werner, J. Chem. Phys. **112**, 3106 (2000).
[39] M. Urban, J. Noga, S. J. Cole, and R. J. Bartlett, J. Chem. Phys. **83**, 4041 (1985).
[40] MOLPRO is a package of *ab initio* programs written by H.-J. Werner and P. J. Knowles, with contributions from R. D. Amos, A. Bernhardsson, A. Berning *et al.*
[41] G. C. Maitland, M. Rigby, E. B. Smith, and W. A. Wakeham, *Intermolecular Forces: Their Origin and Determination* (Clarendon, Oxford, 1980).
[42] A. Degli Esposti and H.-J. Werner, J. Chem. Phys. **93**, 3351 (1990).
[43] E. E. Nikitin and S. Ya. Umanskii, *Theory of Slow Atomic Collisions* (Springer, Berlin, 1984).
[44] V. Aquilanti and G. Grossi, J. Chem. Phys. **73**, 1165 (1980).
[45] V. Aquilanti, P. Casavecchia, G. Grossi, and A. Laganá, J. Chem. Phys. **73**, 1173 (1980).
[46] M. H. Alexander, T. Orlikowski, and J. E. Straub, Phys. Rev. A **28**, 73 (1983).
[47] Z. Ma, K. Liu, L. B. Harding, M. Komotos, and G. C. Schatz, J. Chem. Phys. **100**, 8026 (1994).
[48] A. Nicklass, M. Dolg, H. Stoll, and H. Preuss, J. Chem. Phys. **102**, 8942 (1995).
[49] C. E. Moore, *Atomic Energy Levels* (National Bureau of Standards, Gaithesburg, MD, 1949).
[50] C. H. Becker, P. Casavecchia, Y. T. Lee, R. E. Olson, and W. A. Lester, J. Chem. Phys. **70**, 5477 (1979).
[51] R. H. G. Reid and A. Dalgarno, Phys. Rev. Lett. **22**, 1029 (1969).
[52] F. Pirani and G. Liuti, Chem. Phys. Lett. **122**, 245 (1985).
[53] F. Pirani and F. Vecchiocattivi, Mol. Phys. **45**, 1003 (1987).
[54] P. R. Fontana and R. B. Bernstein, J. Chem. Phys. **41**, 1431 (1964).
[55] T. S. Monteiro and D. R. Flower, Mon. Not. R. Astron. Soc. **228**, 101 (1987).
[56] F. H. Mies, Phys. Rev. A **7**, 942 (1973).
[57] R. H. G. Reid, J. Phys. B **6**, 2018 (1973).
[58] D. M. Neumark, K. R. Lykke, T. Andersen, and W. C. Lineberger, Phys. Rev. A **32**, 1890 (1985).